UNIVERSIDADE DO VALE DO RIO DOS SINOS - UNISINOS
UNIDADE ACADÊMICA DE PESQUISA E PÓS-GRADUAÇÃO
PROGRAMA DE PÓS-GRADUAÇÃO EM GEOLOGIA
NÍVEL MESTRADO

LUIZ FELIPE BERTOLDI DE OLIVEIRA

SYNTHETICSEIS: A SYNTHETIC SEISMIC SOFTWARE

São Leopoldo
2021

O48s Oliveira, Luiz Felipe Bertoldi de.
SyntheticSeis: a synthetic seismic software / Luiz Felipe Bertoldi de Oliveira. – 2021.
15 f. : il. ; 30 cm.

Dissertação (mestrado) – Universidade do Vale do Rio dos Sinos, Programa de Pós-Graduação em Geologia, 2021.
"Orientador: Dr. Paulo Sérgio Gomes Paim
Coorientadora: Dr. Ariane Santos da Silveira."

1. Afloramento. 2. Sísmico. 3. Sismograma sintético. 4. Eclipse Grid. 5. SEG-Y. I. Título.

CDU 55

Dados Internacionais de Catalogação na Publicação (CIP)
(Bibliotecária: Amanda Schuster – CRB 10/2517)

LUIZ FELIPE BERTOLDI DE OLIVEIRA

SYNTHETICSEISMIC: A SYNTHETIC SEISMIC SOFTWARE

Dissertação de Mestrado apresentada ao Programa de Pós-Graduação em Geologia – Área de Concentração, Geologia Sedimentar Linha de Pesquisa Estratigrafia e Evolução de Bacias, da Universidade do Vale do Rio dos Sinos (UNISINOS), como parte das exigências do título de Mestre em Geologia.

Orientador: Dr. Paulo Sérgio Gomes Paim

Coorientadora: Dr. Ariane Santos da Silveira

Banca Avaliadora:

Dr. Roberto Salvador d´Avila

Dr. Sandro José Rigo

São Leopoldo

2021

AGRADECIMENTOS

Aos meus orientadores **Dr. Paulo Sérgio Gomes Paim** e **Dr. Ariane Santos da Silveira** por toda a dedicação e empenho em auxiliar um aluno graduado em computação.

A **PETROBRAS** pela participação no “Projeto Sistemas Continentais - Desenvolvimento de Rotinas Numéricas para Simulação de Sedimentação e Diagênese Siliciclástica e Carbonática”, o qual me propiciou estudar e trabalhar com geologia.

Ao apoio financeiro concedido pela **CAPES/PROSUC** para realização deste mestrado.

Aos colegas do Projeto Continentais que tiveram tanta paciência em me explicar os conceitos de geologia e suas contribuições para elaboração deste trabalho, em especial a **Rudi César Comiotto Modena**.

À minha família, em especial a minha esposa **Rosane Becker Flores** por toda ajuda. Em especial também ao meu irmão **Luiz Ricardo Bertoldi de Oliveira** por suas valiosas contribuições, assim como ocorreu na minha graduação.

Enfim, a todos os amigos que fazem do meu mundo um lugar melhor e me ajudaram na conclusão desta dissertação.

INTRODUÇÃO

Modelos sísmicos sintéticos derivados de estudos de afloramento são úteis para comparação com conjuntos de dados sísmicos reais. Esses modelos permitem aos profissionais de geociências compreenderem como os contrastes gerados pelas mudanças de litologias e os elementos arquiteturais podem ser observados em seções sísmicas.

Para a elaboração desses modelos sísmicos sintéticos normalmente é utilizado a wavelet Ricker e a operação de convolução, processos já difundidos na literatura científica n (Ricker, 1953; Wang, 2015a). Contudo, a concepção de rotinas de computação para a criação desses a partir de um *grid* estratigráfico, requer a compreensão da estrutura de dados utilizadas para o armazenamento de dados de *grids* estratigráficos e arquivos de sísmica SEG-Y (Barry et al., 1975), transformações matemáticas geométricas e como esses recursos devem ser combinados com a wavelet Ricker e o processo de convolução para a geração de um volume sísmico sintético.

Dentro desse contexto, foi desenvolvido como objeto dessa dissertação o software gratuito SyntheticSeis, que permite gerar volumes sísmicos sintéticos a partir do formato de *grid* estratigráfico Eclipse Grid e os parâmetros de resolução sísmica escolhidos pelo usuário do software. O formato do arquivo SEG-Y obtido do software facilita a visualização dos resultados, pois é compatível com diversos softwares com Petrel, Gocad e OpendTect (Emerson, 2020; Schlumberger, 2020; dGB Earth Science, 2020).

Além disso, o software SyntheticSeis foi testado e validado através de um estudo de caso de estratos marinhos profundos do Jurássico expostos na área de Arroyo La Jardinera (Bacia de Neuquén) (Silveira, 2019).

O artigo dessa dissertação foi submetido para a revista “Journal of Applied Geophysics” exatamente como apresentado nesse documento, em duas colunas de texto acompanhando dos arquivos editáveis do artigo em formato Latex.

Highlights

SyntheticSeis: a synthetic seismic software

Luiz Felipe Bertoldi de Oliveira,Ariane Santos da Silveira,Rudi César Comiotto Modena,Luiz Ricardo Bertoldi de Oliveira,Gefersom Cardoso Lima,Paulo Roberto Moura de Carvalho,Paulo Sérgio Gomes Paim

- Open-source software for generation of synthetic seismic volumes
- Data input in Eclipse Grid format (stratigraphic grid) and output in SEG-Y format
- A user-friendly interface
- A seismic view of outcrop and well data

SyntheticSeis: a synthetic seismic software

Luiz Felipe Bertoldi de Oliveira[a,*], Ariane Santos da Silveira[a], Rudi César Comiotto Modena[a], Luiz Ricardo Bertoldi de Oliveira[b], Gefersom Cardoso Lima[b], Paulo Roberto Moura de Carvalho[c] and Paulo Sérgio Gomes Paim[a]

[a]*Graduate Program in Geology, Universidade do Vale do Rio dos Sinos, 93022-000, São Leopoldo, RS, Brazil*
[b]*Graduate Program in Applied Computing, Universidade do Vale do Rio dos Sinos, 93022-000, RS, São Leopoldo, Brazil*
[c]*Centro de Pesquisa da Petrobras - CENPES (PETROBRAS)*

ARTICLE INFO

Keywords:
outcrop
seismic
synthetic seismogram
Eclipse Grid
SEG-Y

ABSTRACT

Synthetic seismic models derived from outcrop studies are useful for comparing with actual seismic data sets. This article presents the software we developed (SyntheticSeis) in terms of its architecture and validation through a complete workflow for the generation of synthetic seismic volume. The SyntheticSeis is an open-source software and its main feature is the easy to use interface for simple interface for creating 3D synthetic seismic volumes from stratigraphic grids in Eclipse Grid files. The SEG-Y file format obtained from the software facilitates the visualization of the results and the software application. The mathematical approach to generate the seismic traces is based on the Ricker wavelet and convolution process. The software was tested through a case study of Jurassic, deep-marine strata exposed in the Arroyo La Jardinera area (Neuquén Basin). The comparison of the synthetic seismic volume with the geological model indicates that software works properly and is reliable. The source code and executable version of the software are available for free on the project website (`https://github.com/feliperails/syntheticseis`).

1. Introduction

Acquisition and processing of three-dimensional (3D) seismic data has enabled the oil industry to increase the efficiency of exploration and production operations significantly (Brown, 2011). On the other hand, the development of realistic 3D geological models of subsurface to obtain statistical relations remains a challenge (Biondi, 2007; Tinker, 1996).

Outcrop analysis is a robust method for identifying the best exploration and production techniques in the hydrocarbon industry. It establishes relationships between the high vertical resolution of wells and the lateral resolution of 3D seismic data. Synthetic seismic models derived from outcrop studies are useful for comparing with real seismic data sets, as well as for determining the origin of seismic reflectors (Janson et al., 2007; Zeller et al., 2015). Besides, outcrop analogues can be used for training seismic interpreters as well as neural networks (Di et al., 2020).

Seismic data mainly helps geophysicists and oil engineers to find new mineral storage and groundwater reservoirs (Apostolou et al., 2007). Other highlights are the computational intelligence techniques used in seismic data processing (Gerolymos et al., 2005).

Seismic modeling allows us to perform subsurface imaging and study seismic attributes (velocities, densities, porosities, amplitudes) of a seismic volume, balance a geological section, perform a time conversion on the seismic section and define/test seismic acquisition parameters in a given area (Rowan and Kligfield, 1989; Xiong et al., 2018).

During the acquisition of seismic data by reflection, a seismic pulse (wavelet) is emitted from a controlled artificial source, and the response is monitored as a function of time. As the wave propagates and reaches the boundary between two layers, some parts of the energy reflect whereas another part propagates further down. The hydrophone devices (or geophones, for the case of land acquisition), positioned on the surface, capture the produced reflections, while the refractions propagate into the deeper regions of the subsurface until they reach a new boundary (Sen, 2006).

The capacity of distinguishing structures in the seismic data relies heavily on the wavelet. This ability is related to the horizontal and vertical resolution of the seismic data (Yuan et al., 2015). If, on the one hand, the capacity is linked to the distance in which two points of reflection need to be separated in order to identify them as distinct points; on the other hand, the vertical resolution is directly linked to the wavelet frequency (Sen, 2006; Kumar et al., 2016).

Although many studies have elaborated 3D synthetic seismograms from outcrop data (Tinker, 1996; Umam, 2002; Bourgeois et al., 2004; Falivene et al., 2010), their elaboration is still created by Matlab scripts or with software that performs only part of the process (Jafarian et al., 2018; Janson et al., 2007; Falivene et al., 2010). Above all, the process of preparing synthetic seismograms based on statistical grids can be complex. Synthetic 3D seismograms are calculated from regular reflectivity grids, whereas statistical grids generally use irregular grids (Caers, 2011; Chen et al., 2020, 2017).

SyntheticSeis is a free, open-source software that provides a simple interface for the creation of 3D synthetic seismic data from stratigraphic grids in Eclipse Grid files and the generation of synthetic seismic volumes in the SEG-Y file format. Both file formats are compatible with different software used by researchers and professionals to create geological models or analyze seismic data (Schlumberger,

*Corresponding author
lbertoldio@unisinos.br (L.F.B.d. Oliveira)
ORCID(s):

2020; Emerson, 2020; dGB Earth Science, 2020; ResInsight, 2020).

The main objective of this article is to show all the functionality of SyntheticSeis and carry out a complete review of the process of creating synthetic seismograms, from the acquisition of velocity data, through the creation of impedance and reflectivity matrices, and the selection of frequencies of Ricker wavelets, to the convolution process. At last, we present a case study, i.e. the application of this tool to the Los Molles Formation, a Jurassic, deep marine succession exposed in the Arroyo La Jardinera region in the southern portion of the Neuquen Basin in central-western Argentina (Silveira, 2019).

2. Mathematical approach of synthetic seismic trace

Scientists realized that seismic waves register important information about earthquakes as well as about Earth´s interior. Therefore, information about those layers can be extracted from the analysis of waves trajectories. Besides shock waves (earthquakes), are artificially produced to create seismic waves to subsurface investigation (Gholamy and Kreinovich, 2014).

This section will cover the mathematical modeling of wavelet and convolution. Both are necessary to generate a synthetic seismic trace that resembles a real post-stack seismic trace.

2.1. Wavelet

The wavelet analysis derives from the needs of the geophysical applications, but it was widely enriched by the contributions of mathematics, engineering, physics and other fields. Wavelet techniques became an important area of research in numerical analysis and advanced signal processing (Wang, 2015a).

Also, wavelets applied to the solutions of partial differential equations provide an alternative tool for developing methods, which enable refinement of the solution according to local regularities. Wavelet analysis has been extensively formalized thanks to the efforts of mathematicians, constituting, but is also a core subject for physicists and engineers, among other professionals.

The Ricker is the second derivative of a Gaussian function, that is, it is symmetric over time. However, seismic signals are often not symmetric, but, instead, are closer to the first derivative of a Gaussian function (Ricker, 1953; Wang, 2015a).

Nevertheless, derivatives of a Gaussian function have similar amplitude spectra, altered from a Gaussian distribution. Therefore, the wavelet is often used in seismic analysis. The amplitude spectrum of Ricker wavelet and the spectra of various derivatives of a Gaussian are asymmetric (Wang, 2014). This equation has a solution based on a particular function of Lambert W (Lambert, 1758; Wang, 2015b). From this function, it is possible to perform an analytical analysis of the frequency bandwidth and the time domain amplitude of the wavelet.

In geophysics, frequency quantities can be used describe seismic resolution, and changes in these quantities can be explored to measure underground attenuation coefficients. However, seismic fields may differ from Ricker's wavelet (Quan and Harris, 1997; Wang, 2015a, 2014).

The Ricker wavelet can be defined as:

$$r(t) = \left(1 - \frac{1}{2}\omega_\rho^2 t^2\right) \exp\left(-\frac{1}{4}\omega_\rho^2 t^2\right), \tag{1}$$

where t is time (in seconds) and ω_ρ is the most energetic frequency (Wang, 2015a; Liu et al., 2004). It is symmetrical in the time domain and has a zero mean, which leads to Equation 2 below,

$$\int_{-\infty}^{+\infty} r(t)dt = 0. \tag{2}$$

2.2. Convolution

A synthetic seismic volume simulates the result captured by geophones of a real seismic volume. Such processes are numerically modeled, giving rise to synthetic data that will be confronted with real data. Input parameters requested at each stage (for example sampling rate, geophone noise rates, number of lines, and crosslines) simulate the original seismic acquisition process.

The convolution operation is defined as the integral of the product of two functions after one of them undergoes a shift in time or space (Sun et al., 2015), as expressed in Equation 3

$$s(t) = \int_{-\infty}^{+\infty} x(\eta) \cdot w(t-\eta)d\eta. \tag{3}$$

Computationally, the integral of Equation 3 represents the sum of the overlapping region of functions x and w, as w moves in relation to x. Equation 4 illustrates the discretization of the convolution operation

$$s(t) = (x \otimes w)(t) = \sum_{\eta=-\infty}^{\infty} x(\eta)w(t-\eta). \tag{4}$$

In the context of convolutional networks, x refers to the set of input images, and w is a set of filters (Sacramento et al., 2018; Zhang et al., 2013; Nose-Filho et al., 2018). The input images are a sequence of data, while the filters are a sequence of parameters to be optimized by the learning algorithm.

This mathematical behavior helps to identify the signal at the origin of a transformation and is commonly used in the seismic study (Russell, 1988; Hatton et al., 1986). Assuming $s(t)$ as the result of the convolution of a reflectivity function of the subsurface layers with the seismic wavelet generated on the surface plus a noise from the acquisition, the convolutional model can be mathematically defined as:

$$s(t) = \omega(t) * \phi(t) + \mu(t), \tag{5}$$

where $s(t)$ represents the seismic signal, $\phi(t)$ is the reflectivity function; $\omega(t)$ represents the wavelet and $\mu(t)$ the noise

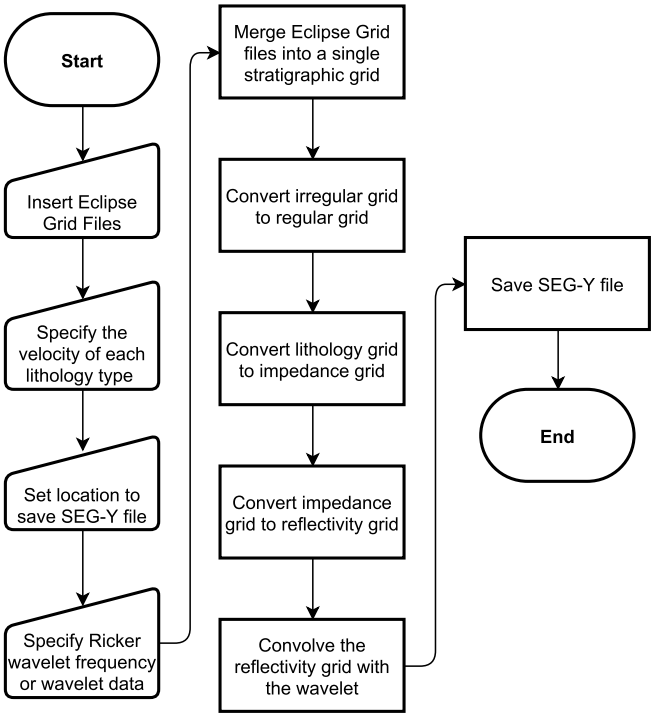

Figure 1: Flowchart of the transformation of a geological model into a synthetic seismic volume using SyntheticSeis.

(all information other than signal). If the noise component is zero, the seismic trace will simply be the convolution of the wavelet with Earth reflectivity (Tarantola, 1984; Ye et al., 2018).

Reflectivity consists of the reflection coefficients for the normal incidence of each time sample. Wavelet being a temporal attenuation function, convolution is the replacement of each reflection coefficient by a scaled version of the wavelet to which it is added the result (Porreca et al., 2018; Wadas et al., 2016).

To obtain the reflectivity function, it is necessary to know the velocities and densities of the subsurface layers, as shown in Equation 6. Therefore, a detailed analysis of the study area is necessary to build velocity and density model. All parameters are based on elapsed time.

$$\phi = \frac{v_2\rho_2 - v_1\rho_1}{v_2\rho_2 + v_1\rho_1} \tag{6}$$

where ϕ is the reflection coefficient, v is the velocity of the ρ-waves in the material, and ρ is its density.

3. The SyntheticSeis Software

SyntheticSeis has several steps to convert a computational geological model into a synthetic seismic volume. The flowchart presented in Figure 1 illustrates the processes performed by this software in order to facilitate the understanding of all the stages involved in the synthetic seismic generation process.

3.1. Irregular Grid to Regular Grid

Geological models can be described by stratigraphic grids that aim to represent complex phenomena in the subsurface. Besides lithologies, major bedding surfaces and fault planes are also indicated (Caers, 2011).

The Eclipse Grid format (GRDECL file) is an irregular stratigraphic grid, specifically a corner-point grid, that stores information about structural and attribute data (Schlumberger, 2014). Corner-point grids are widely used in geological modeling and can be defined as structured grids composed of irregular hexahedrons (Chen et al., 2020, 2017).

The irregular grid of the Eclipse Grid is made up of irregular hexahedral volumes with data corresponding to the geometry of the volumes organized in the COORD and ZCORN sections. Other sections are metadata or are used to associate properties with volumes. These COORD section data correspond to the main layer of the irregular grid (Schlumberger, 2014). An example of the Eclipse Grid file structure is shown in Figure 2 with dimensions 2 on the x -axis, 3 on the y-axis and 4 on the z-axis. With the data from the COORD section a layer of dimensions 2 is formed on the x-axis, 3 on they y-axis and 1 on the z-axis.

The data from the x and y coordinates that make up the main layer are shared with the other layers stacked on the z-axis, as shown in Figure 2. The number of coordinates contained in the COORD section can be defined as:

$$ncv = (ncx + 1)(ncy + 1) \cdot 2 \cdot 3, \tag{7}$$

where ncv is the number of coordinates stored in COORD, ncx is the number of volumes on the x-axis, ncy is the number of volumes on the y-axis, the constant 2 represents the bottom and top vertices, and the constant 3 corresponds to the x, y and z coordinates that are needed to define each of the vertices.

Using the main layer, highlighted in yellow in Figure 2a, the points of each of the eight vertices of the hexahedrons are stored starting by the coordinate with the smallest values of the x- and y-axes, running in the direction of the x-axis and merging the top and bottom vertices of this layer (Figure 2b). Neighboring hexahedrons share vertices, so it is not necessary to save all eight points for each hexahedron, as calculated in Equation 7. In this way, the odd COORD section lines belong to the top of the layer and the even lines to the bottom (Figure 2b and Figure 2c). When all vertices in the direction x-axis are stored, the coordinate value y is increased and the x-axis is traversed again. This process is repeated until all vertices of the main layer are saved in the COORD section. The result for the proposed example can be seen in Figure 2c.

To form the other layers along the z-axis, the ZCORN section shifts the z coordinates of the vertices formed with the COORD section data along the lines formed by the z-axis data contained in ZCORN. The data in the ZCORN section are not shared between the volumes; that is, for each volume of the Eclipse Grid, there are 8 points contained in the ZCORN section. Therefore, the number of coordinates con-

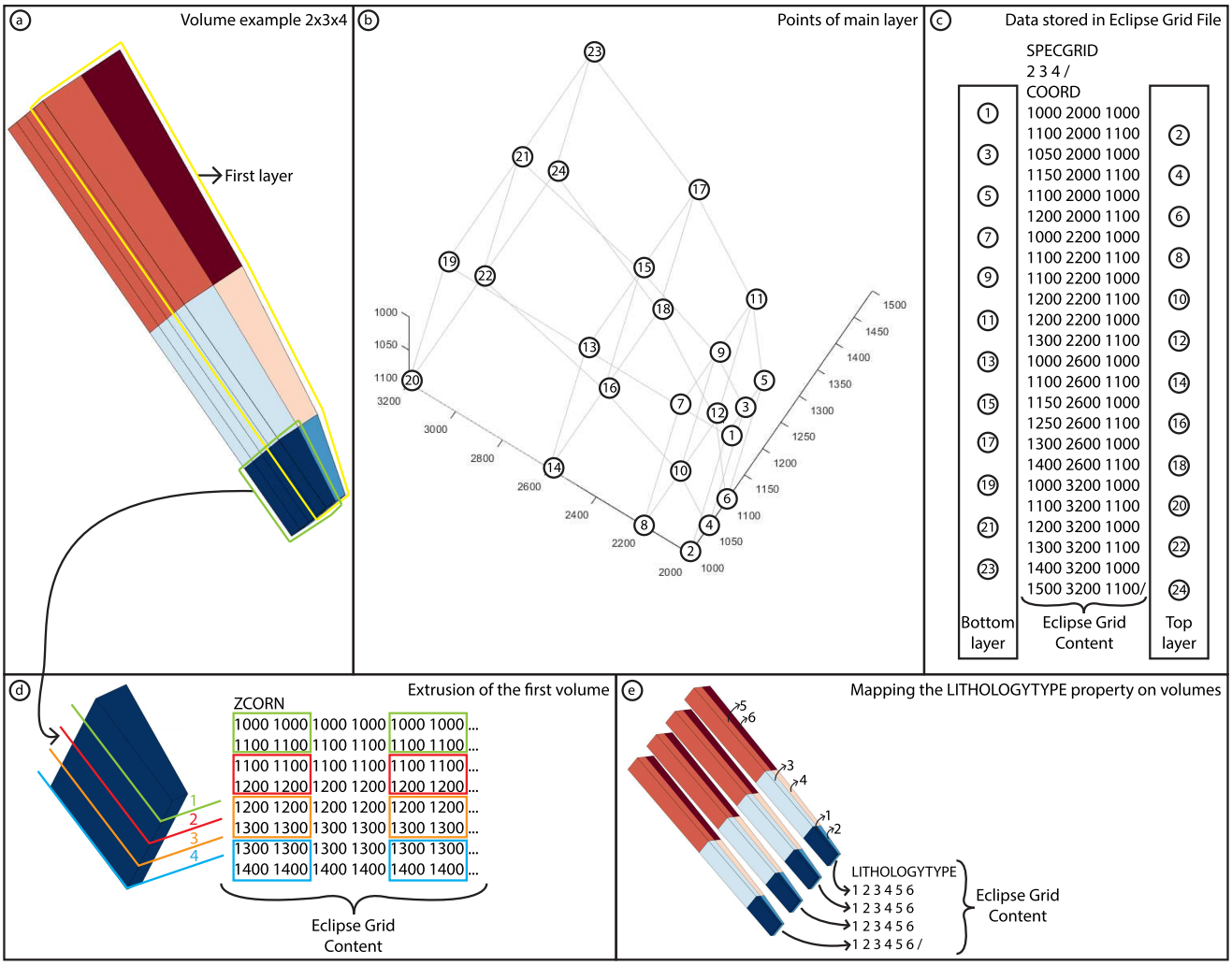

Figure 2: Organization of an Eclipse Grid file in text format. a) Example of an irregular grid with dimensions 2 on the x-axis, 3 on the y-axis and 4 on the z-axis. b) Visualization of the numbering of the hexahedron vertices, taking into account the main layer (highlighted in yellow in Figure 2a). c) Organization of the coordinates of the vertices in the COORD section, where the odd lines represent the top of the hexahedron and the even lines the base. d) Organization of the coordinates of the z-axis of the vertices in the ZCORN section, taking into account the first volume (highlighted in green in Figure 2a). e) Organization of lithology codes in the LITHOLOGYTYPE section.

tained in the ZCORN section can be defined as:

$$nzv = ncx \cdot ncy \cdot ncy \cdot 8, \tag{8}$$

where nzv is the number of coordinates stored in ZCORN, ncx is the number of volumes on the x-axis, ncy the number of volumes on the y-axis, ncz the number of volumes on the z-axis, constant 8 represents the eight coordinates z per hexahedron.

To exemplify how the data are saved in the ZCORN section, we used a volume with 4 hexahedrons that are stacked in the direction of the z-axis,as highlighted in green in Figure 2a. Figure 2d detail the volume used in this example. In the ZCORN and COORD sections, the coordinates of the z-axis of the vertices are stored starting at the smallest coordinate of the y-axis and traversing in the direction of the x-axis. The result is displayed in Figure 2d, where the eight coordinates that make up each of the four volumes are highlighted in different colors. This section follows the same pattern as COORD, where odd lines will be composed by coordinates of the top of the hexahedron and the even ones by the bottom ones.

Finally, we need to map the lithologies corresponding to each volume. By default, the section that stores the type of lithology is LITHOLOGYTYPE, and the mapping on the volumes is as shown in Figure 2e, following the same pattern as the COORD and ZCORN sections. The number of lithological types present in the LITHOLOGYTYPE section is calculated using Equation 9.

$$nl = ncx \cdot ncy \cdot ncy, \tag{9}$$

where nl is the number of lithologies in the LITHOLOGYTYPE section, ncx is the number of volumes on the x-axis,

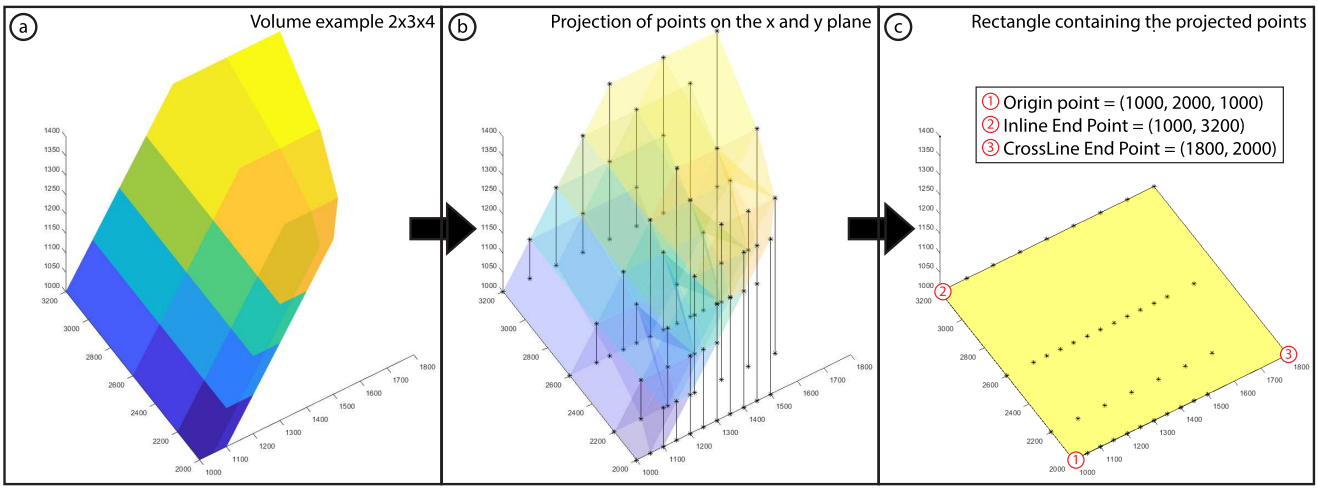

Figure 3: Generation of the minimum rectangle imported from an Eclipse Grid file. a) Same example volume presented in Figure 2a with another position. b) Projection of all hexahedron vertices of the irregular grid in the x-y plane. c) Generation of the smallest rectangle that encompasses all points projected on the x-y plane.

ncy the number of volumes on the y-axis and ncz the number of volumes on the z-axis.

After the previous steps, it is necessary to calculate the hexahedron of the Eclipse Grid mesh, which is formed by eight three-dimensional points and associated lithology. Thus, to calculate a regular three-dimensional grid with rotation in the two-dimensional space of x and y axes and to obtain a maximum resolution with the smallest number of volumes, it is necessary to calculate the minimum rectangle formed by the extracted hexahedrons, as shown in Figure 3.

Although a regular three-dimensional grid with two rotations could further optimize the resolution with a minimum number of volumes, there is no need to calculate the minimum rectangle in the two-dimensional space x and z or y and z, but the SEG-Y file data structure does not support this type of rotation.

Figure 3a shows the same volume as Figure 2a. To calculate the minimum rectangle, the volume in Eclipse Grid has all its vertices projected on the x-y plane (Figure 3b). As shown in Figure 3c, the smallest rectangle that can encompass the points projected on the horizontal plane is obtained. After that, the origin point, inline endpoint, and crossline endpoint are calculated to position the SEG-Y in the three-dimensional space, as represented by points 1, 2, and 3 in Figure 3c.

The algorithm then creates the three-dimensional matrix of the regular grid and associates it with the lithology of each cell, according to the number of cells defined in each of the three-dimensional axes and the hexahedron of the Eclipse Grid. The program user should avoid high resolutions in this step because seismic data have maximum detail in the 30-meter scale; that is, a regular high-quality grid will severely affect the processing time of the program, with no benefits for the final visualization of the synthetic seismic volume.

To associate the lithology data of each cell in the regular grid (Figure 4a), the hexahedron is broken into six irregular tetrahedrons (Figure 4b). For each tetrahedron, the algorithm calculates the cube that limits the three-dimensional space of the tetrahedron and which cells of the regular grid are in the two-dimensional space of that tetrahedron. With the list of these cells, the algorithm then calculates the center of each one according to the minimum rectangle and the number of cells on each axis.

The CGAL (Computational Geometry Algorithms Library) was used. This library is an open-source project for developing graphical algorithms in C++ (The CGAL Project, 2020) that provides data structures and algorithms related to computational geometry. The CgalPolyhedronTree3D class was used to verify that the cell center is contained in the three-dimensional space of the tetrahedron, as shown in Figure 4c.

The cube calculation step is a light computational process compared to the process performed by the CGAL library. However, the latter checks whether the cell center is contained in the tetrahedrons. Without this process, all the cell centers of the regular grid would have to be compared with all the tetrahedrons that form the hexahedrons. To complete the optimization of the algorithm, the processing of the hexahedron is paralleled, respecting the number of cores of the computer's processor.

3.2. Lithology model to seismic data

The synthetic seismic volume was created using the vertical convolutional modeling technique, which considers the seismic trace as the convolution between the wavelet and the reflection coefficients (Sheriff and Geldart, 1995; Yilmaz, 2013). According to Yi et al. (2013), it is possible to subdivide the wavelet estimation methods into two classes, the first one is purely statistical approach whereas the second one incorporates well data and was here adopted.

Steps for synthetic seismic generation are described using an example with hypothetical information of lithologies,

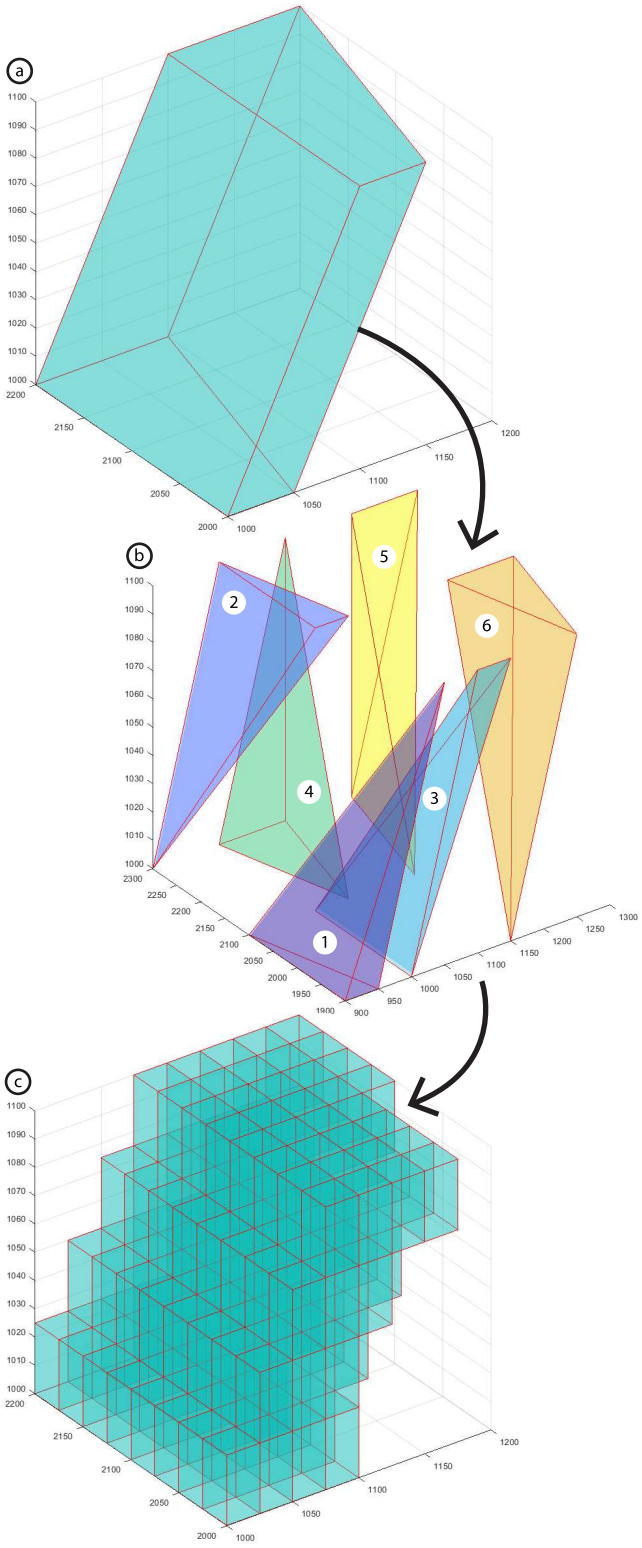

Figure 4: Transformation of an irregular hexahedron into a set of regular hexahedrons. a) First hexahedron of the Eclipse Grid represented in Figure 3a. b) Hexahedron is subdivided into six irregular tetrahedrons. c) Tetrahedrons allow the definition of the hexahedrons of the regular grid, with the support of CGAL, to be used to represent the original volume.

Table 1
Identifiers, lithologies, their associated velocities and densities used to generate the impedance in the example of Figure 5.

Identifiers	Lithologies	Velocity (m/s)	Density (kg/cm^3)
1	Lithology 1	1000	1
2	Lithology 2	2000	1
3	Lithology 3	3000	1

velocities, density, and Ricker wavelet (Figure 5).

The first step consists of the division the regular grid of lithologies into slices parallel to the x coordinate axis. The cell datum for each slice of the regular grid is filled with the lithology of each cell (Figure 5a).

The lithologies, represented by their identifiers, are transformed into impedances by multiplying velocity by density (Figure 5b) along the second step. Velocity and density values are indicated in Table 1.

In the third step, the algorithm generates a matrix for each slice of the grid with the reflectivity coefficients according to Equation 6. As can be seen in Figure 5c, only when there is a lithology change does the reflectivity coefficient differ from zero.

In the fourth step, the program obtains or creates the wavelet to be used in the synthetic seismic trace. SyntheticSeis software has a Ricker wavelet generator with the frequency data defined by the user. The wavelet's sampling degree, that is, how many positions the wavelet will have, is automatically determined according to the size of the regular grid cell on the z-axis, although it can be manually defined by the user. It is also possible to import custom wavelet data from a comma-separated values file (CSV). Figure 5d shows the values of the wavelet used in this example.

Finally, the last step consists of the convolution operation for each column of the reflectivity matrix with the wavelet data determined in the previous step (Figure 5e).

3.3. Seismic data in a regular grid for data organization of the SEG-Y file

SEG-Y files store the seismic trace data in binary format, and the header is stored in Extended Binary Coded Decimal Interchange Code (EBCDIC) (Barry et al., 1975). This requires knowledge of EBCDIC encoding and the organization of trace data in bytes for reading and writing files in this format. Due to this, we use the Segyio Library (ASA, 2019), which resumes the reading and writing layer in SEG-Y files. Segyio is a library in the Python or Matlab programming languages that facilitates interaction with SEG-Y and Seismic Unix files. Although Python is not the most suitable language for processing large volumes of data, the parts that require more processing are implemented by the library core developed in C language, which grants to this library an excellent performance.

With the Segyio library, the program can write the file header by using the Python native text type. The library converts Python's native text encoding to EBCDIC format in a transparent way.

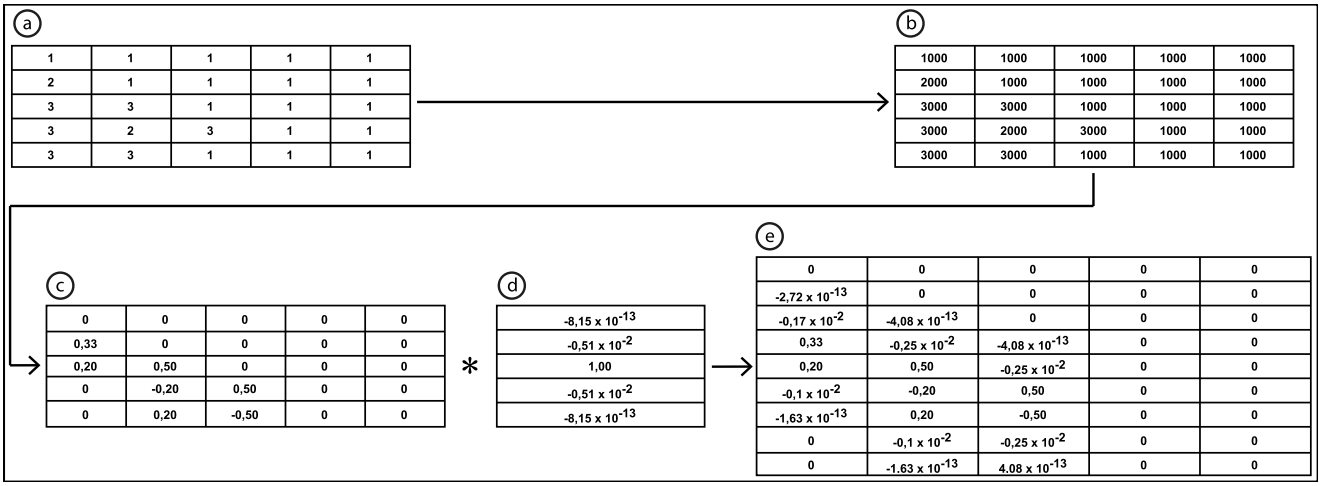

Figure 5: Steps for generating a synthetic seismic section from a hypothetical example. a) Matrix with the lithology identifiers. b) Matrix with the impedance values calculated with data from Table 1. c) Matrix of reflectivities. d) Vector with values referring to the wavelet. e) Resulting synthetic seismic section.

The next step is to record the geometry of the SEG-Y file. It is formed by one of the points of the minimum rectangle plus the adjacent right and top points. Only the origin point has the information of the depth or z-axis information because all other points store only the x-axis and the y-axis values.

Finally, we must organize the three-dimensional matrix data in the form of a two-dimensional matrix that forms the traces of the SEG-Y file. To do it, the algorithm divides the three-dimensional matrix into sections parallel to the two-dimensional space formed by the x and z axes. Therefore forming two-dimensional matrices. These matrices are attached, forming a single two-dimensional matrix of dimension x * y and z.

In summary, we can map the three-dimensional matrix in dashes with the equation:

$$t(i,d) = m\left(\left\lfloor \frac{i}{dimY} \right\rfloor,\ i \bmod dimY,\ d\right), \tag{10}$$

where t represents the trace, i the trace number, d the depth or the z-axis, m the 3D matrix, and $dimY$ the number of cells on the y-axis of the three-dimensional matrix.

That is, the trace of number i in the depth position d is equal to the matrix of the regular grid in position i divided by $dimY$ on the x axis, which is rounded down (floor operator); in the position equal to the rest of the division of i divided by $dimY$ on the y axis; and in position d on the z axis.

4. Case study

This section demonstrates an application of SyntheticSeis in a case study on the Neuquén Basin in Argentina.

4.1. 3D Geological Model

The Arroyo La Jardinera area is located in central-western Argentina, in the southern region of the Neuquén Basin (Figure 6a). The basin has a triangular shape. It is up to 700 km long in the N-S direction and covers an area of 160,000 km^2 (Ramos, 1998). Two large cratonic blocks demarcate its limits: the Sierra Pintada System, to the NE, and the North Patagonian Massif, to the SE (Figure 6a). The Neuquén Basin comprises a thicker than 7,000 m pile of marine to continental sedimentary rocks (Zavala, 2005) recording an interval from the Upper Triassic to the Paleocene (Ramos, 1998).

The studied package belongs to the Jurassic Los Molles Formation of the Cuyo Group and consists of deepwater deposits including expressive channelized and non-channelized turbidites. The Cuyo Group lies on either Pre-Cuyo Group or metamorphic basement rocks (Leanza, 1990). The sedimentary succession starts with a 300m thick transgressive package composed of deep-marine strata (base of the Los Molles Formation). This basal transgressive unit is followed by a thick regressive package that includes 700 m of slope rise through slope to shelf margin deposits (Burgess et al., 2000; Paim et al., 2008, 2011).

This region contains the thickest exposed turbiditic succession in the Neuquén Basin. Paim et al. (2008) subdivided this unit into depositional sequences J1, J21, J22, and J23. According to Gulisano and Gutiérrez-Pleimling (1995) data, this succession encompasses a time interval from 183 to 171.6 Ma (Figure 6c).

The J1 Sequence comprises muddy basin plain facies, minor turbidite lobe fringe deposits, and rare slope rise turbidite lobes strata. Local, intrusive volcanic rocks are also present (Silveira, 2019).

The J21 Sequence is composed of turbidite lobes and interlobes strata and subordinate turbidite channel facies. Turbidites lobes facies range from fine- to coarse-grained sandstones, but medium-grained sandstones are dominant (Silveira, 2019).

The J22 Sequence records the transition from slope to slope rise facies. Turbidite lobes in the slope rise facies

Table 2
Identifiers, lithologies, and their associated velocities used to calculate impedance (Yilmaz, 2013; Schöen, 2015; Silveira, 2019).

Identifiers	Lithologies	Velocity (m/s)
1	Mudstone	2800
2	Siltstone	3000
3	Fine-grained Sandstone	3200
4	Medium-grained Sandstone	3500
5	Coarse-grained Sandstone	3700
6	Very Coarse-grained Sandstone	4000
7	Conglomerate	4500
8	Volcanic	6000

are similar in terms of dimensions and grain size to those recorded in the J21 Sequence. Channel deposits comprise sandstone lenses thinner than 5m (Silveira, 2019).

The J23 Sequence is composed of slope facies, mainly turbidite channels encased within mudstones. Turbidite channels are infilled by sandstones and tend to be wider and thinner towards the base of the slope. Toward the top, they become conglomeratic and tend to be narrower and thicker, occurring either as isolated or amalgamated bodies (Silveira, 2019).

The 3D geological model produced by Silveira (2019) was based on the interpretation of an IKONOS satellite image (Figure 6b) supported by field data (eleven sedimentological logs equivalent to wells). Based on this data set, the SKUA-GOCAD software was used to perform two types of stochastic simulations. At first,the Boolean simulation uses an object modeling technique to determine architectural elements. Then, the Sequential Indicator Simulation (SIS) is used to predict facies in the geological model constrained by the limits defined by the modeled objects (Figures 6b and 6c).

4.2. Data and methods

We generated the synthetic seismic volume using the three-dimensional stochastic facies model of the Los Molles Formation developed by Silveira (2019). This model comprises a volume of 6 km x 12,5 km x 1 km formed by grid of 500 m x 500 m x 5 m cells (x, y, z). The model also presents the simulation of four, about 250 m thick depositional sequences.

Then, we exported the four sequences that make up the 3D geological model to the Eclipse Grid format and, in the SyntheticSeis software, we grouped the files into a single regular grid with 287 inlines (x-axis), 735 crosslines (y-axis), and 1252 samples (z-axis) that is equivalent to a cell dimensions of 20 m x 18 m x 1 m.

Table 2 contains the propagation velocity data in different lithologies used by this case study. We used the numerical codes of the facies as a reference for identifying the lithology velocities, and a velocity of 2500 m/s in the areas around the model to create an impedance contrasts contrast where the geological model region starts.

We then informed the wavelet data required to generate the synthetic seismic volume. In this case, we used the zero phase Ricker wavelet generator to create three synthetic seismic volumes with frequencies of 25 Hz, 40 Hz, and 75 Hz, with a step of 0.46 and no noise.

Finally, the software created SEG-Y files for later viewing in programs such as SKUA-GOCAD™ and OpendTect. We visually validated the three generated synthetic seismic volumes mainly through the evaluation of geometries and Impedance contrasts in relation to the 3-dimensional stochastic facies model.

4.3. Results and interpretations

We here present the results obtained for the case study of the Arroyo La Jardinera region using the SyntheticSeis software with the parameters previously described. The software data entry is a graphic interface with the numerical parameters of the software and the physical locations of the Eclipse Grid files containing the model (Appendix A), and the data output are SEG-Y files of lithologies, acoustic impedances, reflectivity, and synthetic seismic volumes at 25 Hz, 40 Hz, and 75 Hz.

The SEG-Y file of lithologies is important to certify that the dimensions of 287 inlines, 735 crosslines, and 1252 samples (number of cells in depth) were sufficient to reproduce the details in the Eclipse Grid files that contained the model. For this case study, we observe that there are no significant differences between the Eclipse Grid model and the SEG-Y of lithologies (Figure 7a).

In the SEG-Y file of acoustic impedances, see that lithologies with similar acoustic velocities will not be highlighted in the synthetic seismic volume, such as the mudstone of 2800 m/s and the siltstone of 3000 m/s (Figure 7b). In Figure 7c, the acoustic impedance data were transformed into reflectivities, in which it is no longer possible to estimate the volume occupied by the lithologies, only their contacts.

At last, Figure 7d shows some inlines and crosslines of the synthetic seismic volume generated with a 25 Hz Ricker wavelet. It is noticeable that the lithological contacts clearly delineated by their reflectivities (Figure 7c) lose resolution, becoming thicker traces (Figure 7d) in which it is only possible to notice differences between thick lithological packages or related to large acoustic impedance differences.

In order to validate the synthetic seismic volumes, the stratigraphic subdivision of the geological model into four depositional sequences, the architectural elements and major lithological changes were searched and identified in the synthetic seismic volume, following Silveira (2019) procedure. In this way, six geological features present in the inline 6 of lithologies (Figure 8a) were compared with the representations in the synthetic seismic volumes of 25 Hz (Figure 8b), 40 Hz (Figure 8c) and 75 Hz (Figure 8d).

The geological feature 1 represents a volcanic intrusion in the J1 sequence seen in all synthetic seismic sections due to the faster acoustic velocities than the surrounding lithologies (coarse-grained sandstone, mudstone and siltstone). Additionally, the size of the volcanic dyke, about 23m high, fa-

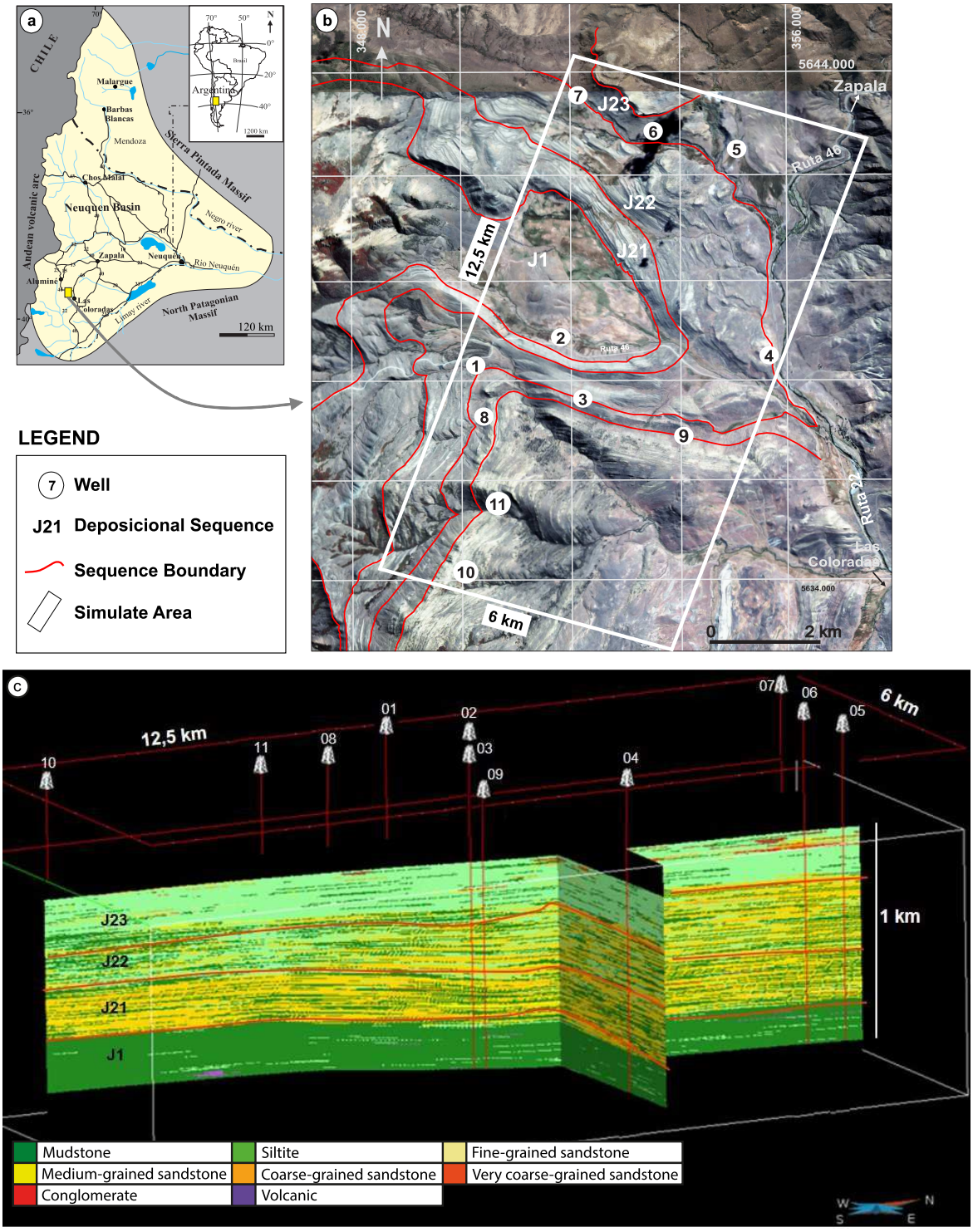

Figure 6: a) Location map of Neuquén Basin in South America; b) IKONOS satellite image, logs location and geological map of the Arroyo La Jardinera area. c) Logs location and 3D stochastic model of lithological distribution along the four depositional sequences (modified from Silveira, 2019).

cilitates its identification in the synthetic seismic section.

The geological feature 2 register the unconformity bounding the J1 and J21 depositional sequences. This boundary is clearly seen and quite well defined along the entire synthetic seismic section due to the lithological contrast between the fine-grained strata of the J1 sequence and the sandier interval that lies on top of it (J21 sequence).

The geological feature 3 comprises extensive sandstone beds associated with turbidite lobes interfingered with finer-grained, thinner bedded lobe fringe strata. These laterally

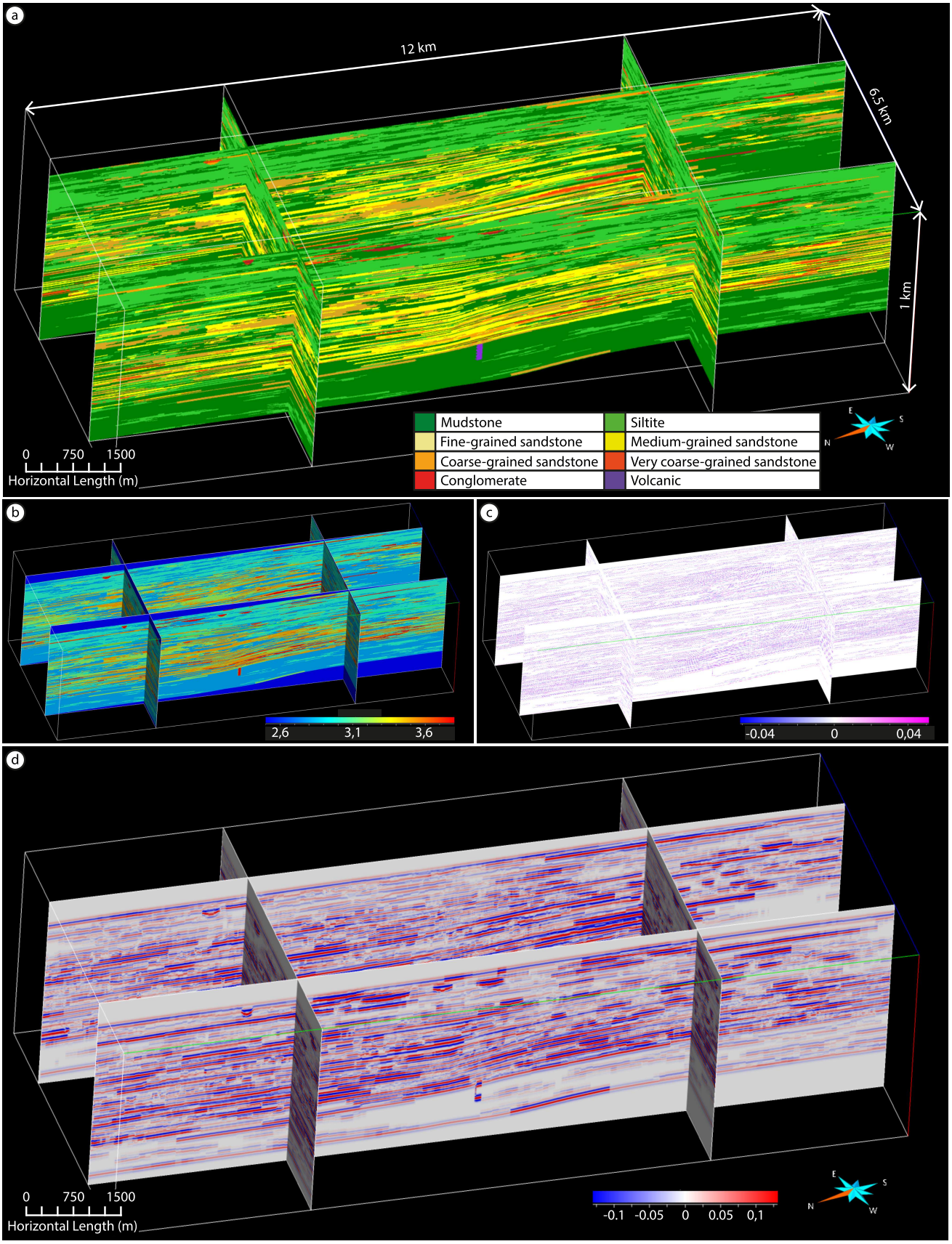

Figure 7: Results of the SyntheticSeis program in SEG-Y format. a) Geological model. b) Acoustic impedances. c) Reflectivities. d) 25 Hz synthetic seismic.

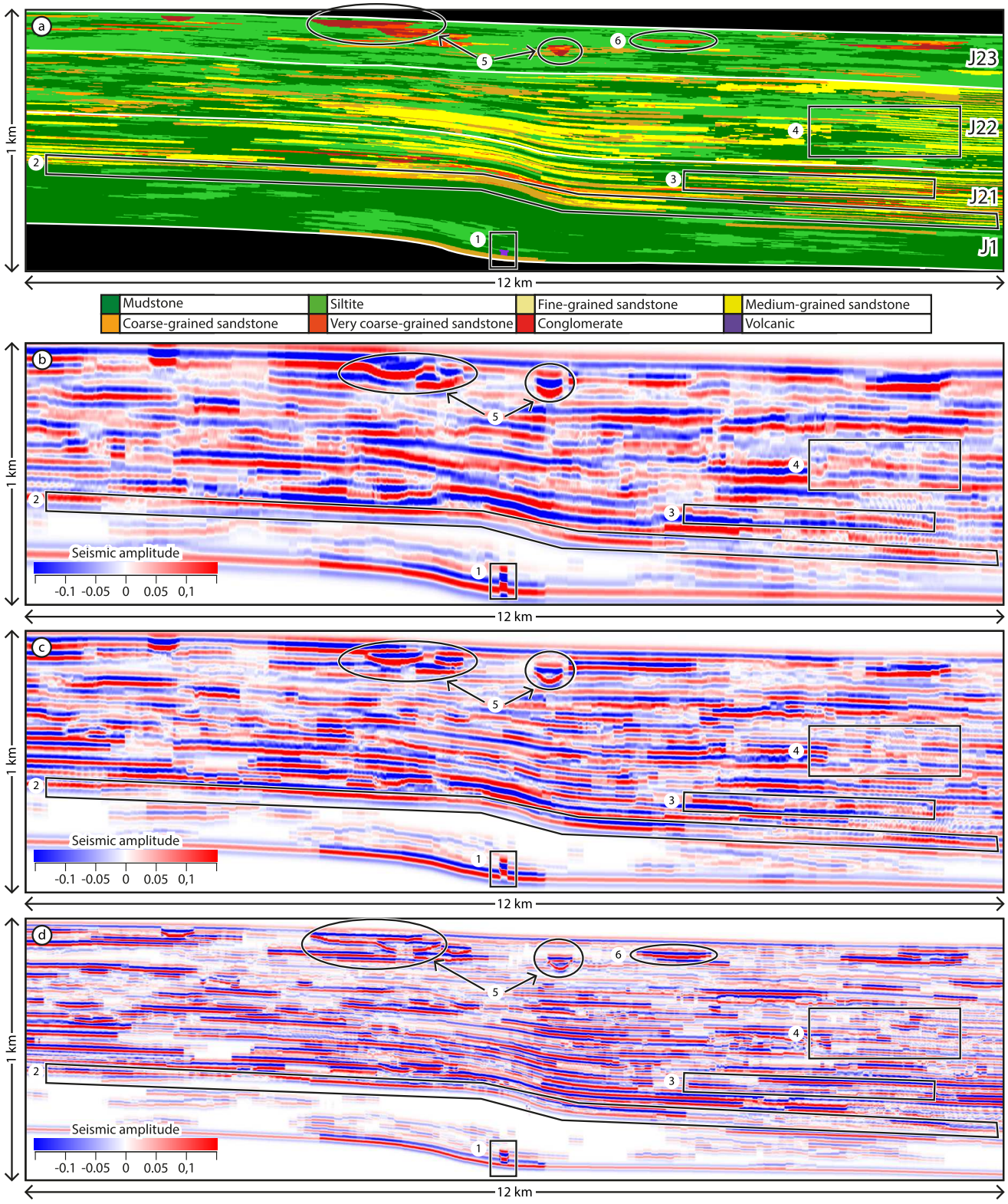

Figure 8: Results presented in longitudinal sections. a) Geological model, highlighting three conglomeratic channels at the top of the model, and an igneous rock intrusion at the base. b) 25 Hz synthetic seismic section. c) 40 Hz synthetic seismic section. d) 75 Hz synthetic seismic section.

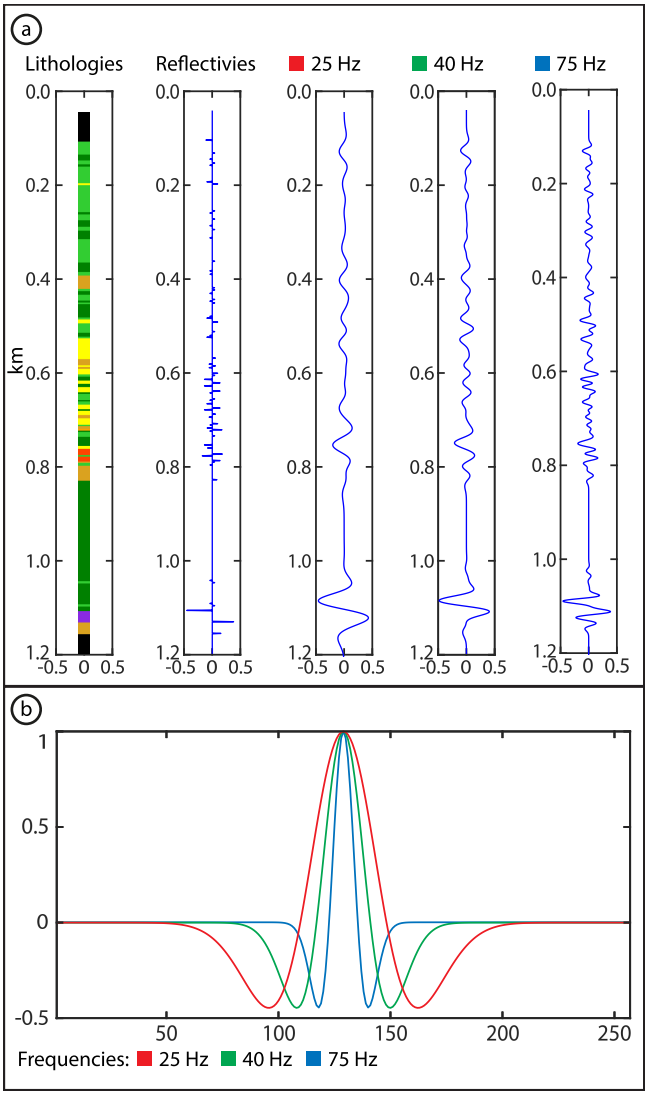

Figure 9: a) Transformation of the inline 6 and crossline 360 profile of lithologies into reflectivities and the 25, 40 and 75 Hz synthetic seismic profiles. The higher the frequency, the more similar the convoluted data are to the reflectivity data. b) Comparison of 25, 40, and 75 Hz wavelets. The longer the wavelength, the lower the frequency, and the result of the synthetic seismogram is distorted relative to the reflectivity data.

extensive sedimentary bodies are quite visible in all synthetic seismic sections (25, 40 and 75 Hz). Another example of the same transition (turbidite lobe to lobe fringe) is presented by the geological feature 4. The lower impedance contrasts, relative to the geological feature 3, make it barely distinguishable in the lower resolution, 25 Hz synthetic seismic section (Figure 8b), but is enough to make it better defined in the higher resolution, 40 and 75 Hz synthetic seismic sections (Figure 8c and Figure 8d).

The geological feature 5 comprises either isolated or amalgamated conglomeratic turbidite channels surrounded by slope mudstones. Lenticular bodies are visible in all synthetic seismic sections in the same position they occur due to the acoustic impedance contrasts between conglomerates (velocity of 4500 m/s) relative to the encasing mudstones (2800 m/s) and siltstones (3000 m/s). Besides, notice that channels internal heterogeneities are more visible as higher the pulse frequency. At last, the geological feature 6 register an isolated, wide sandy channel difficult to recognize in almost all synthetic seismic sections, except in the 75 Hz one where its geometry is observable.

Figure 9a shows the transformation of the lithology trace located in inline 6 and crossline 360 into velocity, reflectivity and synthetic seismic data of 25 Hz, 40 Hz, and 75 Hz. It is possible to notice in the synthetic seismic profile (Figure 9) as well as in the synthetic seismic section (Figure 8) that reflectivity resolution reduces as wavelet frequency decreases.

Comparing the wavelets of the three synthetic seismic volumes, it is possible to realize that the best definition of the synthetic seismic volume of 75 Hz is due to the shortest wavelength of its wavelet. However, high frequency pulses have little practical use as they are not used for acquisition of seismic data for oil and gas exploration due to its relative lower penetration.

5. Discussion

The results obtained using a 3D stochastic model of the Los Moles Formation produced by (Silveira, 2019) who also created a synthetic seismic volume using a private, noncommercial software (FISCAD, a property of Petrobras). However, this program depends on the commercial software GOCAD version 2006, being incompatible with new versions. Therefore, the transformation processes from irregular to regular grid and the creation of the impedance grid must be previously carried out by GOCAD version 2009, or newer, through scripts, which is difficult for unexperienced users.

The implementation of synthetic seismic processing through Matlab has also been previously addressed (Janson et al., 2007; Falivene et al., 2010; Jafarian et al., 2018). However, the advantage of SyntheticSeis is to make available to users a free, open-source software, including commercial use, with a consistent workflow of input and output data. Data entry in Eclipse Grid files facilitates the import of stratigraphic grids created in software such as Petrel (Schlumberger, 2020), SKUA-GOCAD ™ (Emerson, 2020) and the free software ResInsight (ResInsight, 2020). Likewise, SEG-Y output files are compatible for viewing or processing seismic attributes through Petrel, SKUA-GOCAD ™ or the free OpendTect (dGB Earth Science, 2020) software.

Another advantage of SyntheticSeis relative to scripting languages, is that the software is implemented in C++, and its algorithms have been optimized through parallelism techniques offered by the OpenMP (Open Multi-Processing) library (Chandra et al., 2001). For example, the stratigraphic grid presented in this work has approximately 22 million cells in Eclipse Grid files, and after being processed and transformed into a SEG-Y file, the 25 Hz synthetic seismic

volume has about 264 million samples. This volume of data takes a long time to be processed in languages interpreted without compilation like Matlab and Python, even with performance improvements like Matlab's just-in-time (JIT) and Python's Numba (Lam et al., 2015).

Regarding the validation of the results, we observe that the synthetic seismic volumes are in accordance with the chosen settings and frequencies of 25 Hz, 40 Hz, and 75 Hz. The geological features shown in the section of the geological model of lithologies are clear in synthetic seismic sections and represented as in real seismic, excluding noise that is absent in the synthetic seismic process (Figure 8).

SyntheticSeis continues to be constantly developed, with the creation of wrappers for Matlab and Python in order to promote the use of the software keeping the facility of these scripting languages and the speed of C++ processing.

6. Final Remarks

SyntheticSeis was developed to assist researchers in the process of creating synthetic seismic volumes. To validate the software we presented a case study where we show how synthetic seismograms behave using different frequencies of the Ricker wavelet. The software is a free, easy-to-use tool that does not rely on any commercial software or require running complex scripts. Importing stratigraphic grids from Eclipse Grid files gives SyntheticSeis compatibility with the main geological modeling softwares. The updating and addition of new features will be continuous; users are encouraged to suggest improvements, and developers contribute directly to the project's source code.

Acknowledgments

This work was financed through a grant from the Coordenação de Aperfeiçoamento de Pessoal de Nível Superior – Brasil. This research was also supported by Petrobras through the R&D project "Continental Systems Project - Development of Numerical Routines for Simulation of Sedimentation and Siliciclastic and Carbonatic Diagenesis" and by the RING-GOCAD Consortium managed by ASGA that provided the SKUA-Gocad software.

A. Graphic Interface

The synthetic seismic volumes presented in section 4.3 were created using the graphical interface of the SyntheticSeis software. The stratigraphic grids of the J1, J21, J22 and J23 sequences correspond to the files presented in the graphical interface grid_Molles10.grdecl, grid_Molles20.grdecl, grid_Molles30.grdecl, grid_Molles40.grdecl respectively (Figure A.1). Figure A.2 shows the configuration of the quantities of inlines, crosslines and samples of the synthetic seismic volume. Finally, in Figure A.3, the values of velocity and density per lithology are defined, the frequency of the Ricker wavelet, the number of samples of the Ricker wavelet and the path to be saved in the SEG-Y file of the synthetic seismic.

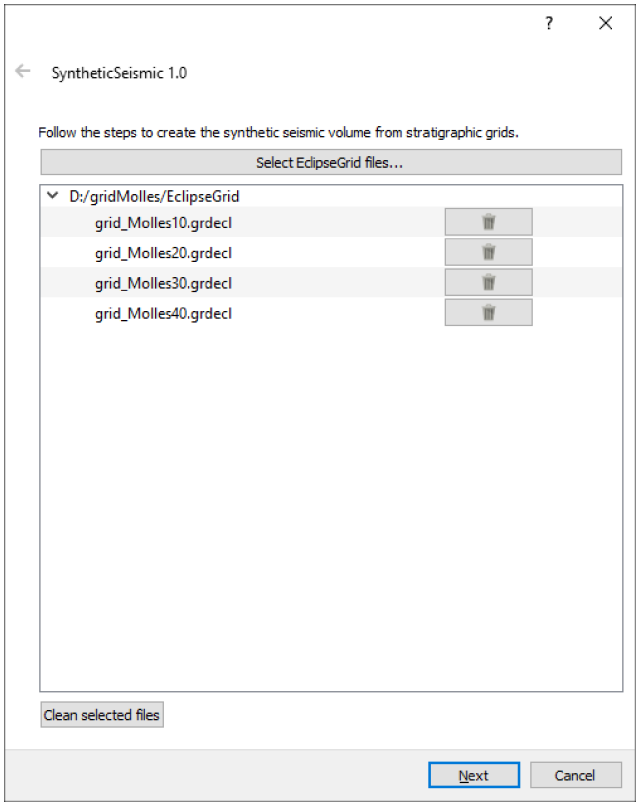

Figure A.1: Graphical interface for adding Eclipse Grid files (stratigraphic grids).

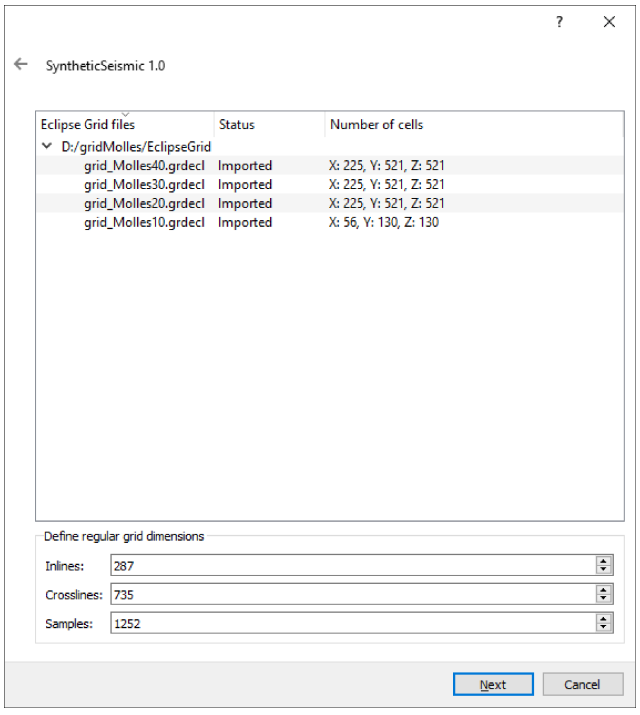

Figure A.2: Graphical interface for configuring the quantities of inlines, crosslines and samples.

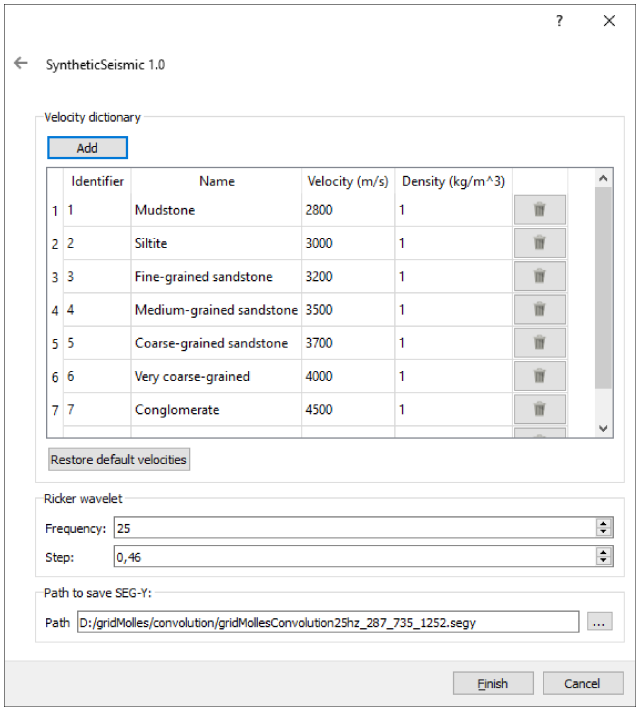

Figure A.3: Graphical interface for configuring velocities, densities and data of Ricker wavelet.

CRediT authorship contribution statement

Luiz Felipe Bertoldi de Oliveira: Conceptualization of this study, methodology, main writing of the manuscript, design and development of algorithms. **Ariane Santos da Silveira:** Geology model, stratigraphy and sedimentology of the case study. **Rudi César Comiotto Modena:** Methodology, review writing and editing. **Luiz Ricardo Bertoldi de Oliveira:** Mathematical approach, review writing and editing. **Gefersom Cardoso Lima:** Software architecture, development of the Eclipse Grid reader and development of graphics components. **Paulo Roberto Moura de Carvalho:** Development of the convolutional model. **Paulo Sérgio Gomes Paim:** Stratigraphy and sedimentology of the case study.

References

Apostolou, M., Gazetas, G., Garini, E., 2007. Seismic response of slender rigid structures with foundation uplifting. Soil Dynamics and Earthquake Engineering 27, 642–654.

ASA, E., 2019. Simple & fast io for seg-y files. 1.9.3 ed. URL: https://github.com/equinor/segyio.

Barry, K.M., Cavers, D.A., Kneale, C.W., 1975. Recommended standards for digital tape formats. Geophysics 486, 344–352. doi:http://dx.doi.org/10.1190/1.1440530.

Biondi, B.L., 2007. Concepts and applications in 3D seismic imaging. Society of Exploration Geophysicists and European Association of ....

Bourgeois, A., Joseph, P., Lecomte, J.C., 2004. Three-dimensional full wave seismic modelling versus one-dimensional convolution: The seismic appearance of the grès d'annot turbidite system. Geological Society, London, Special Publications 221, 401–417.

Brown, A.R., 2011. Interpretation of three-dimensional seismic data. Society of Exploration Geophysicists and American Association of Petroleum ....

Burgess, P.M., Flint, S., Johnson, S., 2000. Sequence stratigraphic interpretation of turbiditic strata: an example from Jurassic strata of the Neuquén basin, Argentina. Geological Society of America Bulletin 112, 1650–1666.

Caers, J., 2011. Modeling Uncertainty in the Earth Sciences. John Wiley & Sons, Ltd. doi:https://doi.org/10.1002/9781119995920.ch8.

Chandra, R., Dagum, L., Kohr, D., Maydan, D., McDonald, J., Menon, R., 2001. Parallel Programming in OpenMP. Morgan Kaufmann Publishers Inc., San Francisco, CA, USA.

Chen, Q., Liu, G., Li, X., Zhang, Z., Li, Y., 2017. A corner-point-grid-based voxelization method for the complex geological structure model with folds. Journal of Visualization 20, 104–404. doi:https://doi.org/10.1007/s12650-017-0433-7.

Chen, Q., Liu, G., Ma, X., Li, X., He, Z., 2020. 3d stochastic modeling framework for quaternary sediments using multiple-point statistics: A case study in minjiang estuary area, southeast china. Computers & Geosciences 136, 104–404. doi:https://doi.org/10.1016/j.cageo.2019.104404.

Di, H., Li, Z., Maniar, H., Abubakar, A., 2020. Seismic stratigraphy interpretation by deep convolutional neural networks: A semisupervised workflow. Geophysics 85, WA77–WA86.

dGB Earth Science, 2020. OpendTect User Documentation - 6.6. https://doc.opendtect.org/6.6.0/doc/od_userdoc/Default.htm.

Emerson, 2020. SKUA-GOCAD software. https://www.pdgm.com/products/skua-gocad.

Falivene, O., Arbués, P., Ledo, J., Benjumea, B., Munoz, J.A., Fernández, O., Martínez, S., 2010. Synthetic seismic models from outcrop-derived reservoir-scale three-dimensional facies models: The eocene ainsa turbidite system (southern pyrenees). AAPG bulletin 94, 317–343.

Gerolymos, N., Apostolou, M., Gazetas, G., 2005. Neural network analysis of overturning response under near-fault type excitation. Earthquake Engineering and Engineering Vibration 4, 213.

Gholamy, A., Kreinovich, V., 2014. Why ricker wavelets are successful in processing seismic data: Towards a theoretical explanation, in: 2014 IEEE Symposium on Computational Intelligence for Engineering Solutions (CIES), IEEE. pp. 11–16.

Gulisano, C., Gutiérrez-Pleimling, 1995. The jurassic of the neuquén basin. a) neuquén province, field guide. Asociación Geológica Argentina E 2, 1–111.

Hatton, L., Worthington, M.H., Makin, J., 1986. Seismic data processing: theory and practice. Technical Report. Merlin Profiles Ltd.

Jafarian, E., de Jong, K., Kleipool, L.M., Scheibner, C., Blomeier, D.P., Reijmer, J.J., 2018. Synthetic seismic model of a permian biosiliceous carbonate–carbonate depositional system (spitsbergen, svalbard archipelago). Marine and Petroleum Geology 92, 78–93.

Janson, X., Kerans, C., Bellian, J.A., Fitchen, W., 2007. Three-dimensional geological and synthetic seismic model of early permian redeposited basinal carbonate deposits, victorio canyon, west texas. AAPG bulletin 91, 1405–1436.

Kumar, R., Das, B., Chatterjee, R., Sain, K., 2016. A methodology of porosity estimation from inversion of post-stack seismic data. Journal of natural Gas science and engineering 28, 356–364.

Lam, S.K., Pitrou, A., Seibert, S., 2015. Numba: A llvm-based python jit compiler, in: Proceedings of the Second Workshop on the LLVM Compiler Infrastructure in HPC (LLVM '15), Association for Computing Machinery, New York, NY, USA. pp. 1–6. doi:10.1145/2833157.2833162.

Lambert, J.D., 1758. Observationes variae in mathesin puram: Acta helvetica: Physico-mathematico-anatomico-botanico-medica. Band III , 128–168.

Leanza, H.A., 1990. Estratigrafía del Paleozoico y Mesozoico anterior a los movimientos intermálmicos en la comarca del Cerro Chachil, Provincia del Neuquén. Revista de la Asociación Geológica Argentina 45, 272–299.

Liu, J., Wu, Y., Han, D., Li, X., 2004. Time-frequency decomposition based on ricker wavelet, in: SEG Technical Program Expanded Abstracts 2004. Society of Exploration Geophysicists, pp. 1937–1940.

Nose-Filho, K., Takahata, A.K., Lopes, R., Romano, J.M.T., 2018. Improving sparse multichannel blind deconvolution with correlated seismic data: Foundations and further results. IEEE Signal Processing Magazine

35, 41–50.

Paim, P.S., Silveira, A.S., Lavina, E.L., Faccini, U.F., Leanza, H.A., Teixeira de Oliveira, J., D'Avila, R.S., 2008. High resolution stratigraphy and gravity flow deposits in the Los Molles Formation (Cuyo Group, Jurassic) at La Jardinera region, Neuquén Basin. Revista de la Asociación Geológica Argentina 63, 728–753.

Paim, P.S.G., Lavina, E.L.C., Faccini, U.F., da Silveira, A.S., Leanza, H., d'Avila, R.S.F., 2011. Fluvial-derived turbidites in the Los Molles Formation (Jurassic of the Neuquén Basin): initiation, transport, and deposition, in: Slatt, R.M., Zavala, C., et al. (Eds.), Sediment Transfer from Shelf to Deep Water: Revisiting the Delivery System, AAPG Studies in Geology 61. AAPG. chapter 5, pp. 95–116.

Porreca, M., Minelli, G., Ercoli, M., Brobia, A., Mancinelli, P., Cruciani, F., Giorgetti, C., Carboni, F., Mirabella, F., Cavinato, G., et al., 2018. Seismic reflection profiles and subsurface geology of the area interested by the 2016–2017 earthquake sequence (central italy). Tectonics 37, 1116–1137.

Quan, Y., Harris, J.M., 1997. Seismic attenuation tomography using the frequency shift method. Geophysics 62, 895–905.

Ramos, V., 1998. Estructura del sector occidental de la faja plegada y corrida del Agrio, cuenca Neuquina, Argentina, in: 10º Congreso Latinoamericano de Geología, pp. 105–110.

ResInsight, 2020. Resinsight post processing of reservoir simulations. https://github.com/OPM/ResInsight.

Ricker, N., 1953. The form and laws of propagation of seismic wavelets. Geophysics 18, 10–40.

Rowan, M.G., Kligfield, R., 1989. Cross Section Restoration and Balancing as Aid to Seismic Interpretation in Extensional Terranes. AAPG Bulletin 73, 955–966. URL: https://doi.org/10.1306/44B4A2BC-170A-11D7-8645000102C1865D, doi:10.1306/44B4A2BC-170A-11D7-8645000102C1865D.

Russell, B.H., 1988. Introduction to Seismic Inversion Methods. Society of Exploration Geophysicists. URL: https://doi.org/10.1190/1.9781560802303, doi:10.1190/1.9781560802303.

Sacramento, I., Trindade, E., Roisenberg, M., Bordignon, F., Rodrigues, B.B., 2018. Acoustic impedance deblurring with a deep convolution neural network. IEEE Geoscience and Remote Sensing Letters 16, 315–319.

Schlumberger, 2014. ECLIPSE Reference Manual Version 2014.1. Schlumberger.

Schlumberger, 2020. Petrel software. https://www.software.slb.com/products/petrel.

Schöen, J., 2015. Physical Properties of Rocks - Fundamentals and Principles of Petrophysics. 2 ed., Elsevier, Amsterdam.

Sen, M.K., 2006. Seismic inversion. Society of Petroleum Engineers Richardson, TX.

Sheriff, R.E., Geldart, L.P., 1995. Exploration seismology. Cambridge University Pres, Cambridge.

Silveira, A.S., 2019. Modelo estocástico e volume sísmico sintético de depósitos turbidíticos de águas profundas: um exemplo da Formação Los Molles, Grupo Cuyo - região sul da Bacia de Neuquén, AR. Tese de doutorado. Universidade do Vale do Rio dos Sinos. São Leopoldo.

Sun, J., Cao, W., Xu, Z., Ponce, J., 2015. Learning a convolutional neural network for non-uniform motion blur removal, in: Proceedings of the IEEE Conference on Computer Vision and Pattern Recognition, pp. 769–777.

Tarantola, A., 1984. Inversion of seismic reflection data in the acoustic approximation. Geophysics 49, 1259–1266.

The CGAL Project, 2020. CGAL User and Reference Manual. 5.1.1 ed., CGAL Editorial Board. URL: https://doc.cgal.org/5.1.1/Manual/packages.html.

Tinker, S.W., 1996. Building the 3-d jigsaw puzzle: Applications of sequence stratigraphy to 3-d reservoir characterization, permian basin. AAPG bulletin 80, 460–484.

Umam, M.S., 2002. Seismic modeling of deepwater outcrop analogs. Ph.D. thesis. Colorado School of Mines.

Wadas, S.H., Polom, U., Krawczyk, C.M., 2016. High-resolution shear-wave seismic reflection as a tool to image near-surface subrosion structures–a case study in bad frankenhausen, germany. Solid Earth 7, 1491–1508.

Wang, Y., 2014. Stable q analysis on vertical seismic profiling data. Geophysics 79, D217–D225.

Wang, Y., 2015a. Frequencies of the ricker wavelet. Geophysics 80, A31–A37.

Wang, Y., 2015b. The ricker wavelet and the lambert w function. Geophysical Journal International 200, 111–115.

Xiong, W., Ji, X., Ma, Y., Wang, Y., AlBinHassan, N.M., Ali, M.N., Luo, Y., 2018. Seismic fault detection with convolutional neural network. Geophysics 83, O97–O103.

Ye, Q., Mei, L., Shi, H., Camanni, G., Shu, Y., Wu, J., Yu, L., Deng, P., Li, G., 2018. The late cretaceous tectonic evolution of the south china sea area: An overview, and new perspectives from 3d seismic reflection data. Earth-science reviews 187, 186–204.

Yi, B.Y., Lee, G.H., Kim, H.J., Jou, H.T., Yoo, D.G., Ryu, B.J., Lee, K., 2013. Comparison of wavelet estimation methods. Geosciences Journal 17, 55–63. doi:https://doi.org/10.1007/s12303-013-0008-0.

Yilmaz, O., 2013. Seismic data analysis: Processing, inversion, and interpretation of seismic data. Geosciences Journal 17, 55–63. doi:https://doi.org/10.1007/s12303-013-0008-0.

Yuan, S., Wang, S., Luo, C., He, Y., 2015. Simultaneous multitrace impedance inversion with transform-domain sparsity promotion. Geophysics 80, R71–R80.

Zavala, C., 2005. Tracking sea bed topography in the Jurassic: the Lotena Group in the Sierra de la Vaca Muerta (Neuquén Basin, Argentina). Geologica Acta: an international earth science journal 3, 107–118.

Zeller, M., Reid, S.B., Eberli, G.P., Weger, R.J., Massaferro, J.L., 2015. Sequence architecture and heterogeneities of a field–scale vaca muerta analog (neuquén basin, argentina)–from outcrop to synthetic seismic. Marine and Petroleum Geology 66, 829–847.

Zhang, H., Wipf, D., Zhang, Y., 2013. Multi-image blind deblurring using a coupled adaptive sparse prior, in: Proceedings of the IEEE Conference on Computer Vision and Pattern Recognition, pp. 1051–1058.